Research Article

Divyanshu Aggarwal*, Vinod Kumar and Siddharth Sharma

Development of Mg-based metal matrix biomedical composites for acicular cruciate ligament fixation by reinforcing with rare earth oxide and hydroxyapatite – A mechanical, corrosion, and microstructural perspective

https://doi.org/10.1515/secm-2022-0179
received July 12, 2022; accepted December 14, 2022

Abstract: This study provides an insight into the synthesis of high-strength and corrosion-inhibiting Mg-based biodegradable implant material by the addition of rare earth oxide material for acicular cruciate ligament reconstruction applications. The matrix has been reinforced with a naturally occurring mineral, hydroxyapatite ($Ca_5(PO_4)_3OH$) and rare earth oxide, neodymium oxide (Nd_2O_3), in different concentrations. The mechanical response has been assessed by analyzing the samples' microhardness, ultimate compressive, and tensile strength. In contrast, the corrosion rates were calculated using phosphate buffer saline solution by using different techniques under suitable physiological conditions. The microstructure characterization has been carried out by field emission scanning electron microscope, electron dispersive spectroscopy, optical microscopy, and X-ray diffraction techniques. Moreover, the surface properties of the composites were assessed using surface roughness and contact angle measurements. The sample showed maximum hardness at a concentration of 1.5% rare earth oxide. Moreover, the highest ultimate compressive and tensile strength followed the same order, i.e., 1.5% > 2% > 1%. In addition, the microstructure analysis revealed a refined microstructure and the formation of secondary intermetallic phases. Resistance to dislocation and grain growth barricading were the prominent features highlighted in the study for enhanced mechanical and corrosion properties. Moreover, the hydrogen evolution was lower for Mg–HA–1.5Nd_2O_3 samples, which was a clear indication of a reduced corrosion rate.

Keywords: magnesium–rare earth oxide composite, mechanical strength, corrosion

Abbreviations

ACL	anterior cruciate ligament
ACLR	ACL reconstruction
EDS	electron dispersive spectroscopy
FESEM	field emission scanning electron microscope
HAP	hydroxyapatite
Mg	magnesium
Nd_2O_3/NdO	neodymium oxide
REO	rare earth oxide
XRD	X-ray diffraction

1 Introduction

The past decade has witnessed the need for advanced biomaterials in the field of orthopedics due to the increase in several bone injuries, and problems like osteoarthritis, osteogenesis, etc. One of the most common knee injuries leading to subsequent knee failure and a high risk of osteoarthritis is an anterior cruciate ligament (ACL) tearing. The patients must undergo ACL reconstruction (ACLR) surgeries to provide stability to the bone surrounding tissues to

* **Corresponding author: Divyanshu Aggarwal,** Department of Mechanical Engineering, Thapar Institute of Engineering and Technology, Patiala, 147004, Punjab, India,
e-mail: divyanshuaggarwal95@gmail.com
Vinod Kumar: Department of Mechanical Engineering, Thapar Institute of Engineering and Technology, Patiala, 147004, Punjab, India
Siddharth Sharma: Department of Biotechnology Engineering, Thapar Institute of Engineering and Technology, Patiala, 147004, Punjab, India

re-establish knee functioning and reduce osteoarthritis progression [1]. Only a 75% success rate has been observed in ACLR, and most failures were due to technical and biological factors [2].

Extensive research has been performed to develop a therapeutic graft to mitigate bone–graft junction healing [3]. The conventionally available implant materials such as Ti alloys, stainless steel, and Ni-based alloys have been utilized for the same. However, unfortunately, their high strength (strength should be 20–140 MPa for UCS, and 30–165 MPa for UTS) exceeds that of the natural bone, leading to a stress-shielding effect and reduction in the bone healing process [4]. To ameliorate such problems, researchers across the globe are focusing on synthesizing new-generation biodegradable implant materials with excellent corrosion resistance and strength. Figure 1 depicts a pictorial view of ACL fixtures and related materials utilized. Mg and its alloys highlighted splendid biocompatibility and strength within the range of natural bone, which reduces stress-shielding effects and several other structural problems. Subsequently, various reinforcing materials have been in the queue to enhance the corrosion resistance properties of Mg alloys and composites due to their inability to survive the corrosion environment. Further, the stress-shielding effect produced by the other metal implants can be mitigated by the use of Mg owing to its density and other mechanical properties that are identical to those of natural bone [5].

Reinforcing materials majorly used include metals, non-metals, and polymers. However, rare earth elements are currently in the limelight as exceptional strength inhibitors and corrosion resistors [6]. The capability to form multiple eutectic phases of rare earth metals assists in increasing the strength of the alloy/composite [6]. Solid solution strengthening and precipitation hardening are the most prominent reasons behind the improved strength of MgRE alloys/composites [7]. In addition, Mg–RE alloys serve as one of the most promising materials in the biomedical industry as a novel biodegradable implant material. This improves the composite's degradation process, leaving no implant residues, and improves the material's strength to survive the physiological environment [8]. However, the major problem in using RE materials is their solubility in the matrix. Excess addition can lead to high agglomeration and inhomogeneity in the materials.

Of all the other RE metals, Nd has the highest solubility in the Mg matrix with a eutectic temperature of 552°C [9]. Chia et al. [9] studied the effects of the addition of La, Ce, and Nd on the Mg matrix and detected the presence of a hard Mg_3Nd phase. Nd served as a better reinforcing material when compared to La and Ce. Knapek et al. [10] reported that WN43 alloy consisted of Mg–4wt% Y–3wt% Nd alloy using spark plasma sintering. This shows that the sintering temperature plays an essential role in the development of secondary phases. This research introduced an optimum temperature of 500°C for better mechanical and

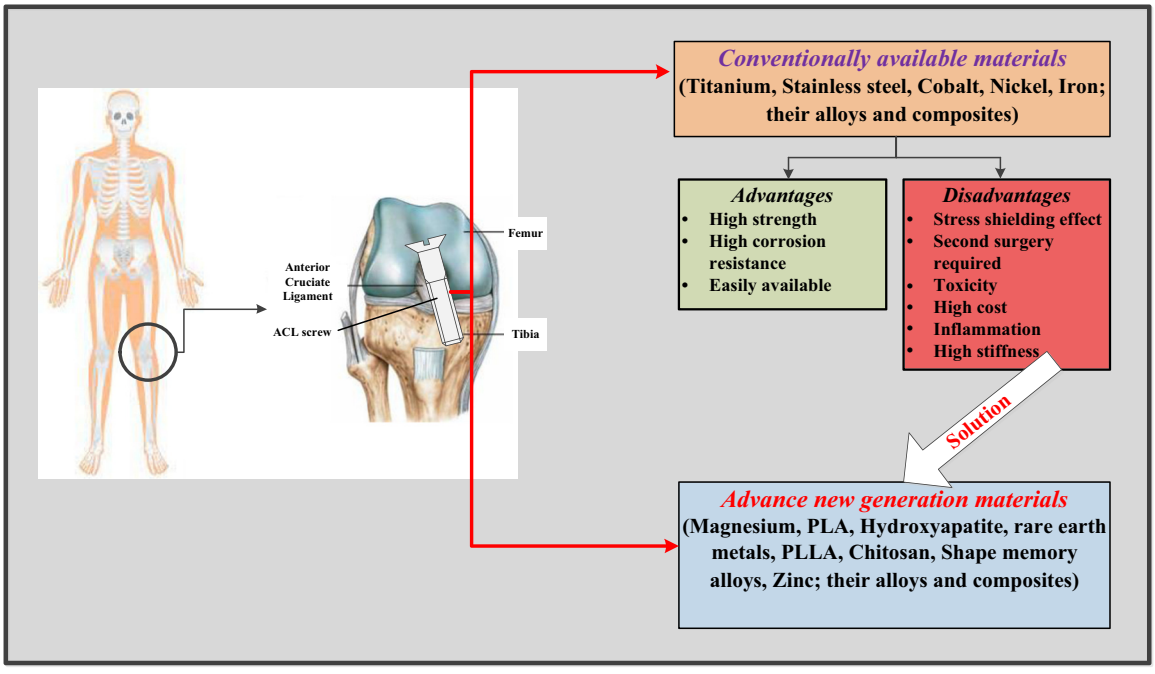

Figure 1: A pictorial view representing the ACL fixation and its implant materials.

microstructural properties. In addition, many studies showcased the use of natural mineral-based ceramic materials, i.e., hydroxyapatite (HAP), as a splendid reinforcing material. The addition of this natural material reduces the chances of toxicity and improves the matrix mechanical and corrosion properties of the matrix [11].

The current study focused on utilizing the oxide form of Nd metal, i.e., neodymium oxide (Nd_2O_3), as a novel reinforcing element. The addition of rare earth oxide (REO) is not new to the research world. These are a special class of materials that are thermally stable metal oxides and have the tendency to reduce the effect of reactive elements due to their strong rare earth–oxygen interactions [12]. In the proposed study, neodymium oxide (NdO/Nd_2O_3), after sintering, produced several eutectic phases, including those developed by adding pure Nd at a lower temperature. This reduces the need of sintering the Mg-matrix at a temperature above their sintering temperature, which may reduce the strength of the matrix. In addition, several mechanical and corrosion properties were assessed, along with the microstructural behavior. The REO has been added in different wt% to determine the optimum concentration for the composite.

2 Research significance

The proposed material is based on the introduction of rare earth metals into the biomedical sector, especially focusing on biodegradable implants. The metals such as Mg, Fe, and their alloys have the tendency to degrade in the physiological environment after a certain time. However, they lack strength and are highly corrosive in nature, leading to early implant failure. Therefore, the current study focuses on improving implant longevity by fabrication of an Mg-based biodegradable implant with the incorporation of HAP and the rare earth metal, i.e., neodymium oxide. The addition of rare earth oxide will provide the necessary strength and corrosion resistance against the physiological environment. Hence, keeping in mind the above objective, several studies have been performed to validate the material's significance for the proposed application.

3 Materials and methods

3.1 Materials

Magnesium (Mg) in powder form, with a particle size of 0.1 mm, was obtained from Fine Laboratory Chemicals, Mumbai, India. The neodymium oxide (Nd_2O_3) powder, with a particle size of 5–7 μm, was purchased from Subra Scientific Company, India. The HAP ($(Ca_{10}(PO_4)(OH)_2)$) powder with an average particle size of 10 μm was purchased from Sigma Aldrich, USA.

3.2 Synthesis of materials

The as-received powders were mixed using a high-energy ball mill (Star Scientific Instruments, India) with a rotation speed of 120 rpm for 2 min, followed by compaction under a Hydraulic pellet pressing machine (PCI analytics, India, maximum capacity of 15Tonne) with a load of 250 MPa. The compacted samples were then placed under a tubular furnace (Antslab, India) for sintering purposes. The sintering time was 2 h at 400°C. The samples were prepared with a size of 13 mm × 5 mm and were then kept grounded with the help of emery paper (300 grit, 1,500 grit, and 2,000 grit) to develop a clean and polished surface. The description of the samples is provided in Table 1.

3.3 Microstructural studies

The synthesized samples were cleaned with distilled water and placed in a vacuum oven for a few hours for microstructure characterization. The samples were kept in a vacuum oven to avoid unnecessary atmospheric contaminations and reactions as well as any moisture contents. Different characterization techniques were utilized to reveal the microstructure of fabricated composite samples. A field emission scanning electron microscope (FESEM) coupled with electron dispersive spectroscopy (EDS) (ZEISS, Sigma 500, Germany) was used for determining the microstructural information of the composite samples. In addition, the X-ray diffraction (XRD) technique (Malvern Panalytical, UK) was used to analyze the intermetallic secondary components developed in the composite samples. A nickel filter and CuK radiation at a voltage of 40 kV with a step size of 0.0131 were used for testing the samples.

Table 1: Description of the samples prepared in the study

Sample	HAP in wt%	Nd_2O_3/NdO in wt%	Mg in wt%
MH1N	10	1	Balance
MH1.5N	10	1.5	Balance
MH2N	10	2	Balance

The data obtained using the XRD technique were analyzed using X'PERT-PRO software and respective peaks were identified. Moreover, the grain structure was analyzed using the optical Microscopy technique (ZEISS, Germany).

3.4 Mechanical properties

The mechanical properties of the composite samples were assessed through three different methods, i.e., microhardness, ultimate tensile strength (UTS), and ultimate compressive strength. The microhardness of the samples was analyzed using a Vickers microhardness tester (Metatech Industries, India) with a diamond indenter and a dwell time of 20 s. The samples were subjected to finishing processes using different grades of emery paper (500, 1,200, and 1,500) before the experiment to develop a clear indentation mark for generating the respective microhardness values. The tensile test was performed using a ZwickRoell tensile tester machine, Germany, with a capacity of 10 kN. The developed samples were of the size 45 mm × 10 mm × 10 mm, and the displacement rate was taken as 0.5 mm/min. Moreover, the compressive strength analysis was carried out on an automatic compression testing machine (AIMIL instrumentation and technologies) with a strain rate of 8.29×10^{-5} s^{-1}. All readings were taken thrice to have reproducibility of results, and finally, the average values were considered.

3.5 Surface studies

To anticipate the change in surface properties due to heat treatment of the fabricated composites, a surface roughness tester (Mitutoyo, SJ400, Japan) was employed. All the composite samples went through similar surface finishing processes for analyzing mechanical properties as in Section 3.4. Afterward, the samples were placed under the experimental setup consisting of a diamond indenter that moved to and fro over the sample. The measuring range was set up to be 800 µm, and the samples were tested in triplicates. The surface hydrophobicity was calculated by determining the contact angle using the sessile drop method (Easy Drop, Kruss, Germany). A total of 20 readings were taken, and finally, the average values were plotted.

3.6 Corrosion studies

The corrosion rates of the developed samples were determined using an immersion test in a phosphate buffer saline (PBS) solution. The corrosion rate of the solid composite samples was determined by equation (1). In addition, the hydrogen evolution (mL/cm^2) was also determined by placing an inverted burette over the test sample, as shown in Figure 2. The burette was filled with PBS solution up to a certain limit. As hydrogen is light in weight, it is collected at the top of the burette and tries to push the solution downwards. The change in volume of the gas was then recorded by measuring the amount of space occupied by the gas in the burette. The corrosion rate was also determined by the electrochemical polarization technique. To perform the electrochemical measurements, the samples were saturated in a three-electrode cell containing PBS solution at 37°C and pH 7.3. The auxiliary electrode was considered as a platinum electrode and the saturated calomel electrode as a reference electrode. The polarization studies were conducted at a scan rate of 0.5 mV/s with a potential range of −0.25 to 1.5 V. The corrosion current of the developed composites was obtained by the Tafel exploration curve. The corrosion rate was calculated using the following equation:

$$\text{Corrosion rate } (C_r) = \frac{2.1\,\Delta m}{A \cdot t}, \tag{1}$$

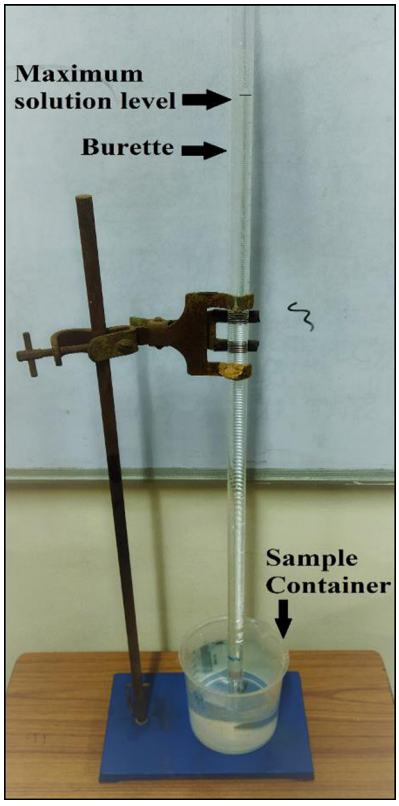

Figure 2: Schematic of the hydrogen evolution measurement setup.

$$\text{Corrosion rate } (C_r) = 3.27 \times 10^{-3} \frac{I_{corr} EW}{\rho}, \quad (2)$$

where C_r is the corrosion rate (mm/year), Δm is the change in weight (mg), A and t are the surface area of the samples (cm^2) and immersion time (days), respectively, I_{corr} is the corrosion current density (mA/cm^2), EW is the equivalent weight of the composite samples, and ρ is the density of materials (g/cm^3).

4 Results and discussion

4.1 Microstructural characterization

Microstructural studies were performed on the samples to analyze the effect of different heat treatment temperatures on the synthesized samples. Figure 3 represents the FESEM images of the samples. A refined surface was achieved after sintering at 400°C for 2 h. When the analysis was observed based on different compositions of NdO, the composite samples consisting of 1.5% NdO showed better intermetallic bonding with the matrix forming a strong and refined structure. The development of crystallographic disorder occurs when NdO is heated at higher temperatures [13]. Due to this, when the synthesized composite with a 1.5% concentration of NdO was heated to a temperature above 400°C, it showed a distorted structure and a higher amount of crystallographic disorder. Moreover, a higher amount of agglomeration was seen over the surface due to inhomogeneity in the matrix pool, forming a divorced eutectic phase $Mg_{12}Nd$ in the crystal lattice. Figure 4 shows the XRD micrograph images of the composite sample, highlighting the formation of secondary intermetallic and divorced eutectic phases. As Mg was the highest in quantity, it showed peaks at 38, 40, 44, and 64°. The HAP, the second-highest in concentration, showed peaks at 48.5 and 69.1°. Some other minor peaks of $Nd_{0.5}Ca_{0.5}$ and $CaCO_3$ were also observed at 71.2, 91.25° and 58, 62°, respectively.

As the alloying content increased up to 1.5%, there appeared to be more fine grains in the microstructure, as shown in Figure 5. But, as the concentration increased above 1.5%, coarse grains started forming, leading to a bimodal grain structure. Therefore, it can be assessed that the composite samples attained well-refined and low defect microstructure when the percentage of NdO was 1.5% as compared to other concentrations. Different components in the developed composites with their respective

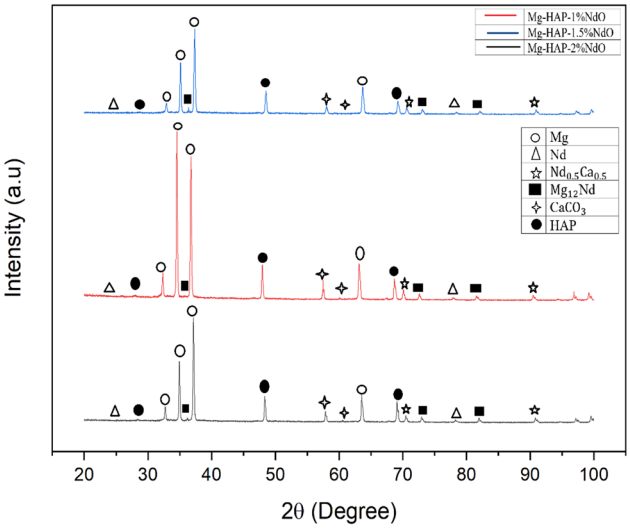

Figure 4: X-ray diffraction results of the composite samples.

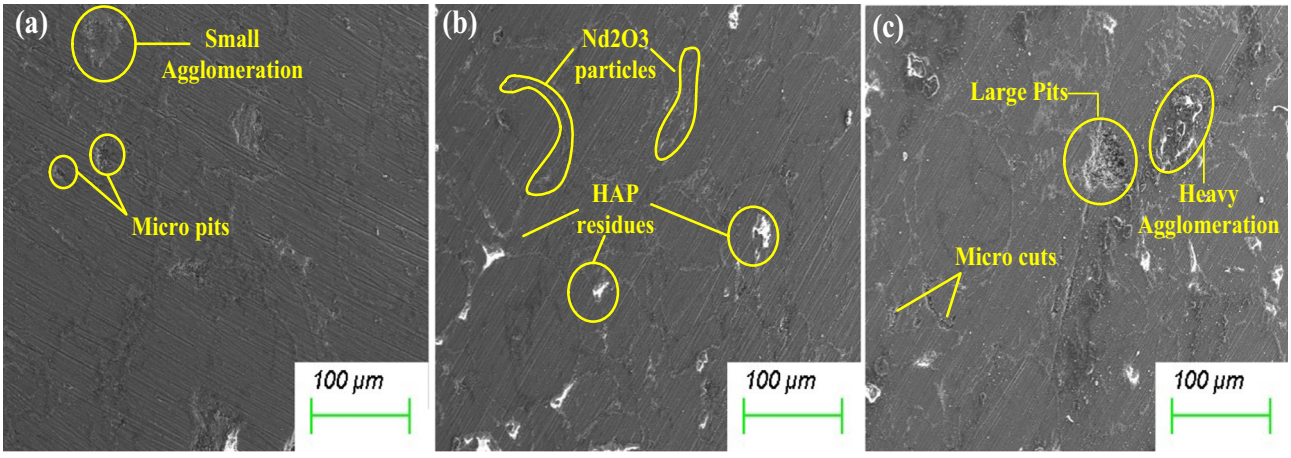

Figure 3: FESEM microstructure images of (a) MH1N, (b) MH1.5N, and (c) MH2N.

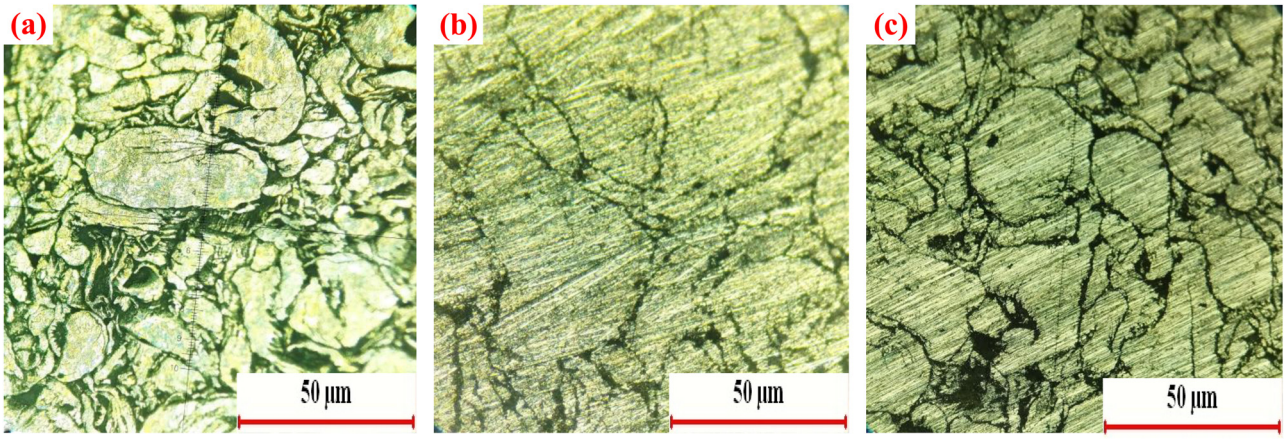

Figure 5: Optical micrographs showing the microstructures of (a) MH1N, (b) MH1.5N, and (c) MH2N.

concentrations available after heat treatment can be observed in EDS microscopic images in Figure 6.

4.2 Mechanical properties

Figure 7(a) represents the developed microhardness values of the composite samples. The test revealed an increase in the composite's hardness with the addition of rare earth oxide. Microhardness was improved in the order of %age reinforcement addition, i.e., 1.5% > 2% > 1%. Herein, the sample MH1.5N depicted a maximum hardness value of 47.48 HV, whereas MH2N and MH1N attained a microhardness of 38.941 and 33.72 HV, respectively. Typically, the microhardness values of cortical and cancellous bone are in the range of 35–40.38 HV and 35.18–40 HV, respectively [14]. Hence, the addition of a rare earth oxide into the Mg matrix pool successfully generated a microhardness value that is within the range of natural bone. The addition of 1.5 wt% NdO and 10 wt% $Ca_{10}(PO_4)(OH)_2$ hard particulates induced a brittle behavior at some regions that resisted the indentation and increased the hardness. However, when the concentration of NdO increases above 1.5%, the microhardness tends to decrease, which can be due to heavy agglomeration over the surface of the sample due to the inhomogeneous distribution of particles over the composite. Whereas with the addition of 1.5% rare earth, the divorced eutectic phase $Mg_{12}Nd$ developed due to incomplete solubility of Nd particles in the matrix; it gets distributed across the grain boundaries. This hinders the dislocation movement and directly strengthens the Mg matrix. Similar results were obtained when Nd was added to the Gr/Al composite with a varying percentage of 0.2, 0.5, and 2 wt% [15].

Similarly, the experiment performed to analyze the UTS showed that the composite sample MH1.5N dominated the other samples with UTS and UCS values of 154.23 and 116.87 MPa, respectively. The UCS value of natural bone lies in the range of 100–200 MPa for the cortical bone and 0.1–16 MPa for the cancellous bone, with a UTS value in the range of 50–151 MPa for the cortical bone [16]. The results are shown in Figure 7(b). According to the Hall–Petch relation, the primary reasons for improved strength were solid solution strengthening and refined grain structure that lead to enhanced strength. In addition, the development of secondary β-eutectic phases and distribution of reinforcing particles across the grain boundaries provided a resistance to the dislocation movements following the Orowan loop mechanism. Similar mechanisms for strengthening the Mg matrix were seen with the addition of Nd and Zn as reinforcing elements [17]. Figure 7(c) represents a combined pictorial view differentiating the strength and hardness results of the three composites in a single view. It shows that the MH1.5N composite sample covered the maximum region with MH1N having a minimum area compared to pure Mg. Hence, the combination of different strengthening mechanisms due to the addition of rare earth oxide and natural mineral ceramic HAP improved the microhardness, UTS, and UCS values of the synthesized composites.

4.3 Surface properties

The surface properties of the composite sample developed were analyzed using two different properties. Figure 8 represents the surface roughness of the samples, and Figure 9 shows the change in surface hydrophobicity by

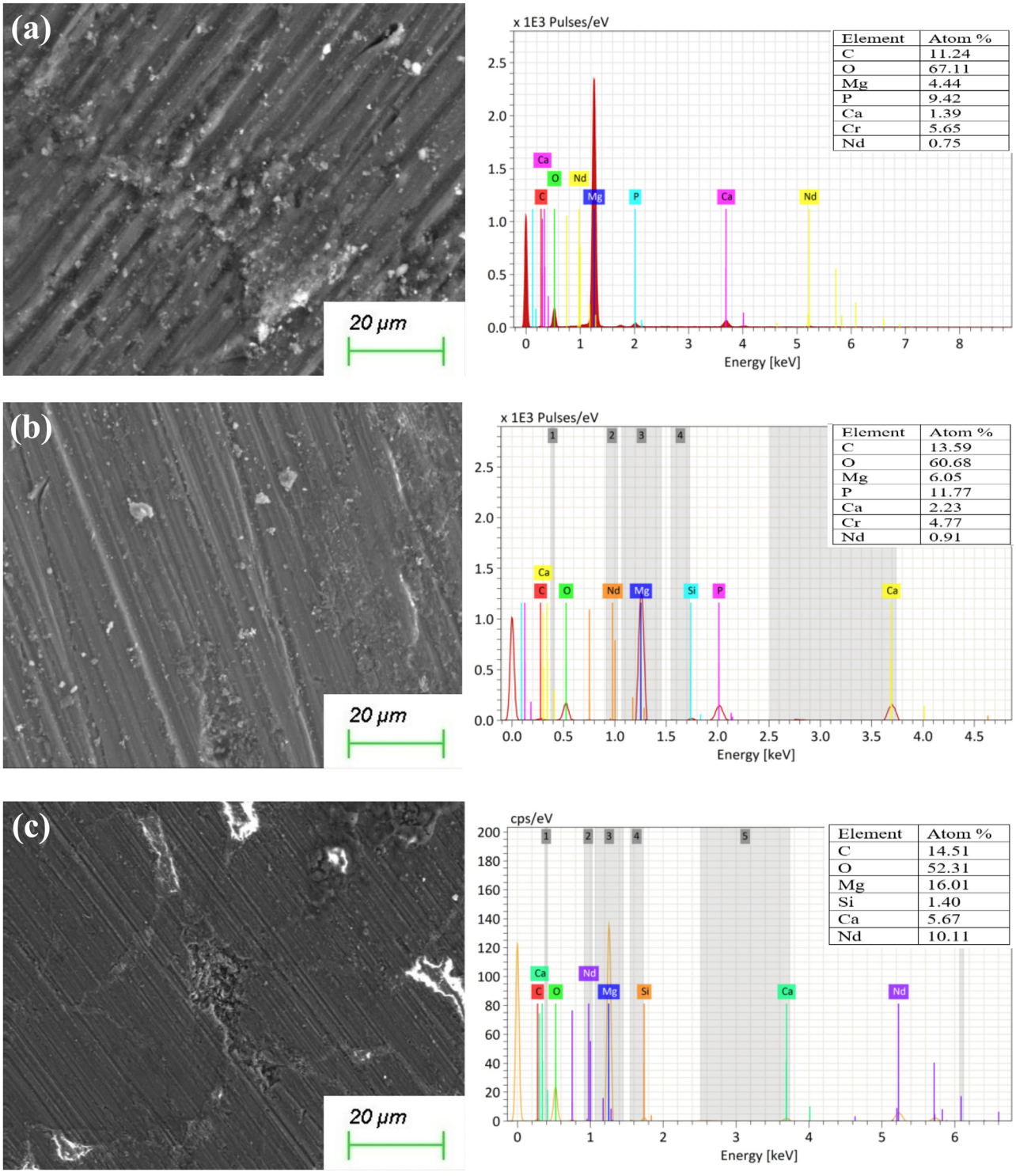

Figure 6: EDS results of (a) MH1N, (b) MH1.5N, and (c) MH2N.

contact angle analysis due to the change in the %NdO concentration. As highlighted under the FESEM and optical microscopic studies, sample MH1.5N performed splendidly by producing a refined and defect-free surface with an average surface roughness (R_a) of 0.24 µm. However, heavy agglomeration was spotted when the percentage concentration of NdO reached above 1.5%, with the sample MH1N showing an average R_a value of 2.29 µm. In addition, large pits and several micro-cuts were available over the surface, increasing the surface roughness. The average surface

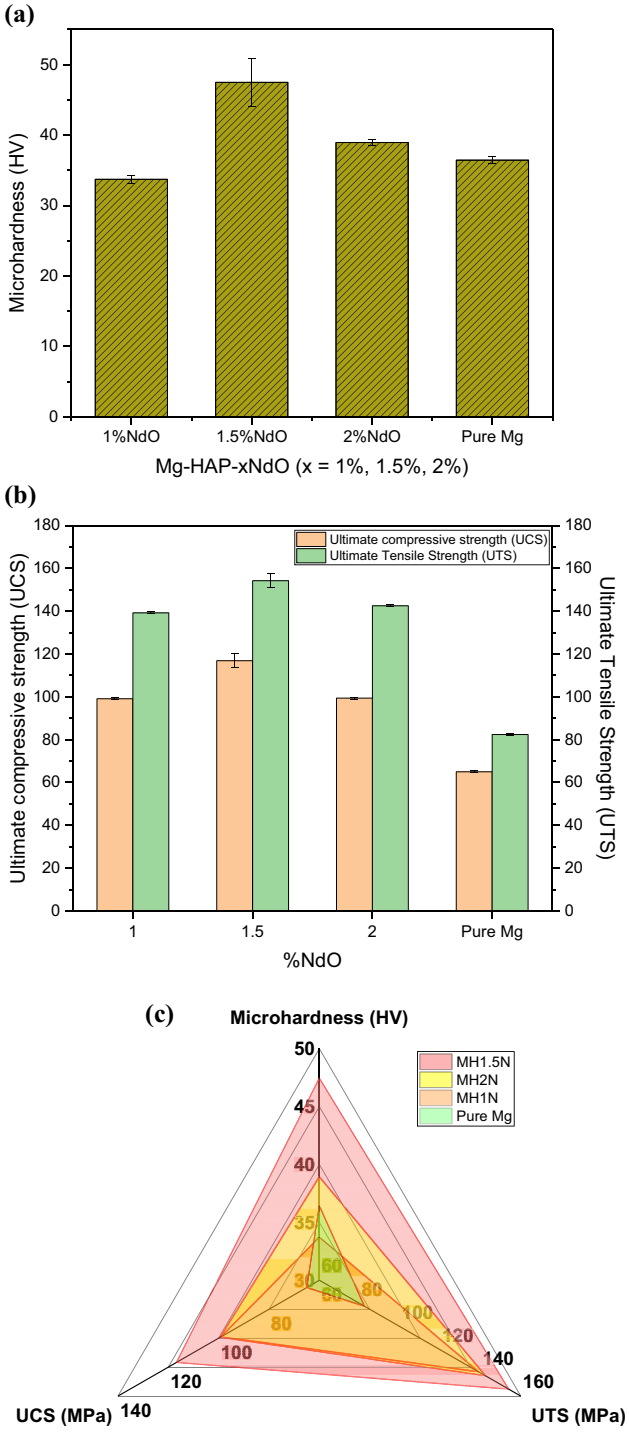

Figure 7: Graphical representations of (a) Vicker's microhardness results and (b) ultimate tensile and ultimate compressive strength. (c) Comparison between the mechanical properties of developed composites (data for pure Mg acquired from refs. [33,34]).

roughness for the composite sample MH2N was observed to be 0.30 µm, slightly higher than that of MH1.5N but lower than that of MH1N. This can be due to smaller pits and low agglomeration compared to the MH1N sample, which reduced the R_a of the MH1N sample. In addition, as seen from the optical microscope images, samples MH1N and MH2N consist of several gaps between the grains as well as many holes, causing intergranular cracking. Due to this, when the diamond probe of the surface roughness tester was allowed to slide over the surface, it started penetrating inside the cracks, increasing the R_a value. Therefore, when the water droplet was dropped over the sample during contact angle analysis, it was seen to enter the pores and cracks available on the surface. Hence, the contact angle values were reduced and the hydrophilicity of the composite samples increased. By contrast, the hydrophobicity also increases with an increase in surface roughness [18]. However, in the current study, the principal reason for the increase in surface roughness was the presence of extensive intergranular cracks and micropores. Nonetheless, the sample MH1.5N showed the lowest roughness along with the minimum surface cracking due to the water drop retention. This resulted in improved surface hydrophobicity, thereby increasing the contact angle value for the MH1.5N composite sample.

4.4 Corrosion rate

The corrosion rate of the developed composite was analyzed using different methodologies. During immersion in a corrosion medium, the Mg samples undergo different chemical reactions that lead to the sample's corrosion. In general, during Mg corrosion, a hydroxide layer is formed when it reacts with water molecules of the corrosion media as per equation (2). This process results in the evolution of hydrogen gas. The evaluation of hydrogen gas is an essential aspect of analyzing the corrosion rate of implant material. A higher amount of hydrogen release can lead to the development of gas pockets around the tissue, increasing the surrounding pH level and decreasing the healing effect [19].

$$Mg + 2H_2O \rightarrow Mg(OH)_2 + H_2, \quad (2)$$

$$Mg \rightarrow Mg^{2+} + 2e^-, \quad (3)$$

$$2H_2O + 2e^- \rightarrow H_2 + 2OH^-, \quad (4)$$

$$Mg^{2+} + 2OH^- \rightarrow Mg(OH)_2, \quad (5)$$

$$Mg(OH)_2 + Cl^- \rightarrow MgCl_2 + OH^-. \quad (6)$$

It can be observed from Figure 10(a) that the current density of MH1.5N (26.40 µA/cm^2) is quite lower than those of MH1N (43.40 µA/cm^2) and MH2N (35.9 µA/cm^2); the order of corrosion rate was MH1.5N (0.505 mm/year)

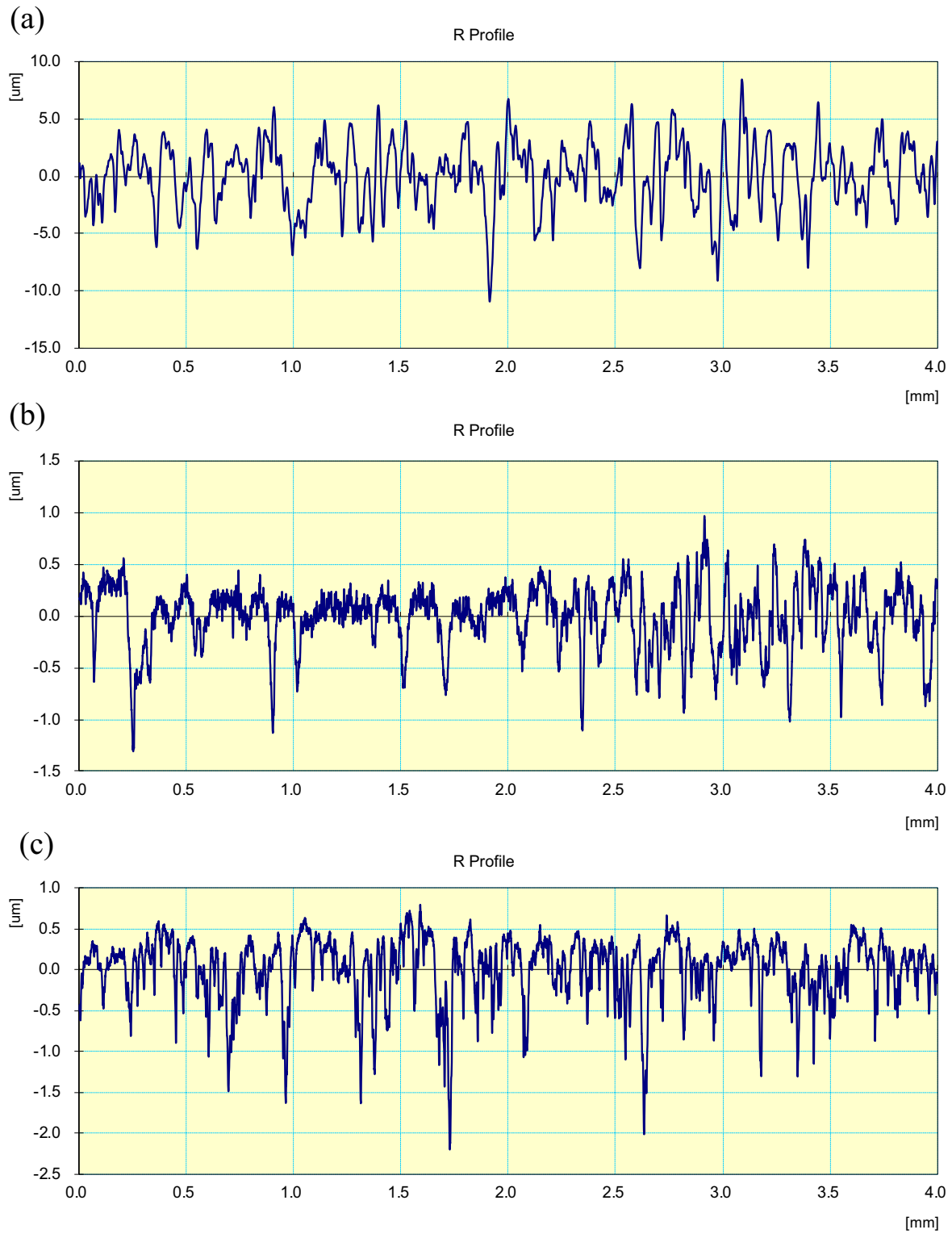

Figure 8: Surface roughness measurement of the microstructure of (a) MH1N, (b) MH1.5N, and (c) MH2N.

<MH2N (0.727 mm/year) <MH1N (0.808 mm/year), as shown in Table 2. The corrosion rates of the composite samples determined through the weight-loss method were seen to be in the same order: MH1.5N (0.146 mm/year) < MH2N (0.431 mm/year) < MH1N (1.425 mm/year). The corrosion rate analyzed through the two tests showed a similar

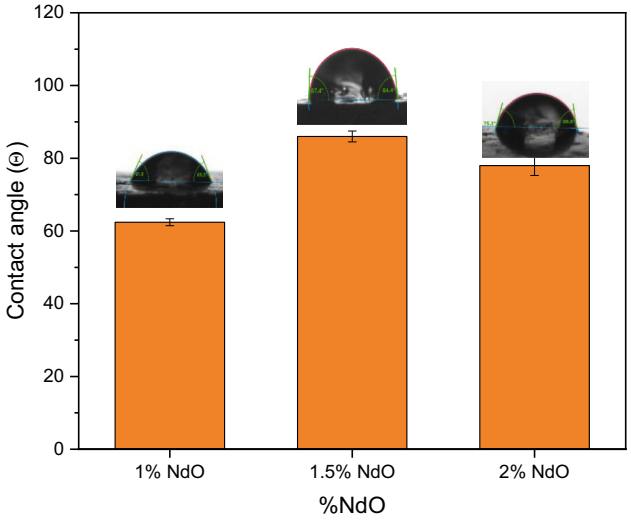

Figure 9: Graphical representation of the contact angle analysis by the sessile drop method.

variation in values for all three composite samples. The weight-loss method provides an average result of the samples in the corrosion media over a certain time interval, whereas the electrochemical method provides instantaneous results of corrosion rates [12]. Therefore, the C_r values obtained by the electrochemical polarization method were higher as compared to those obtained by the weight loss technique. Figure 10(b) represents the corrosion rates of the proposed composites using two different methods. It can be seen that Mg1.5N showed minimum corrosion rates as compared to other samples in all the test methods. The ideal corrosion rate for the Mg-based material should be less than 0.5 mm/year [20]. Therefore, the developed composites in the current study successfully outclassed the standard range, with MH1.5N showing the lowest corrosion rate values.

It can be seen from Figure 10(c) that the hydrogen evolution increased with time, with the MH1.5N sample showing the lowest release rate of 1.2 mL/cm^2. Simultaneously, the change in pH was seen to enhance during initial immersion days but became stable afterward. The principal reason for corrosion resistance was the corrosion barrier provided by the secondary eutectic phases developed. The corrosion was primarily seen as intergranular; therefore, the formation of divorced eutectic phases Mg12Nd and the HAP microparticles between the grain boundaries immensely resisted the corrosion. These phases were seen to be less in the MH1N and MH2N composite samples. The $Mg(OH)_2$ layer developed over the sample during the initial reaction stage was not able to withhold the Cl^- ions for a longer time, as shown in equation (6),

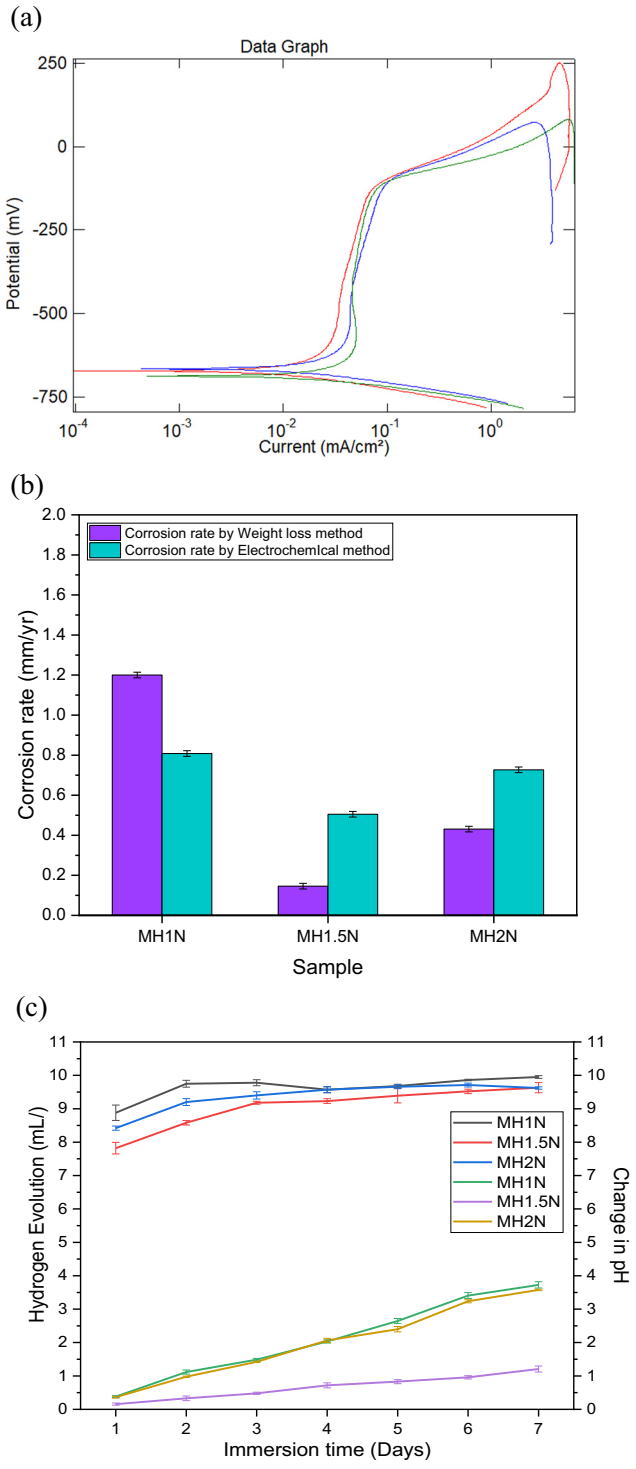

Figure 10: Image showing (a) potentiodynamic polarization curves and (b) corrosion rate (C_r) calculated by the weight loss and electrochemical methods. (c) Hydrogen evolution and change in the pH of the synthesized composite.

resulting in the catalytic degradation of the samples. However, the reinforcing compounds developed in the

Table 2: Corrosion rate values of the composite samples determined by the electrochemical and weight loss experiments

Sample	I_{corr} (μA/cm^2)	C_r (electrochemical test) in mm/year	C_r (weight loss method) in mm/year
MH1N	43.404 ± 1.013	0.808	1.425
MH1.5N	26.401 ± 1.231	0.505	0.146
MH2N	35.908 ± 1.559	0.727	0.431

composites forming hard intermetallic structures provided significant corrosion resistance.

5 Conclusions

In the current study, the author developed cold-pressed Mg–HAP–*x*neodymium oxide (MH*x*N) composites sintered at 400°C for 2 h for orthopedic applications. The mechanical, corrosion, surface, and microstructure properties were assessed, and the following conclusions were drawn:

1. FESEM and optical microscopy images showed refined microstructures with XRD data depicting the development of secondary eutectic $Mg_{12}Nd$, $Nd_{0.5}Ca_{0.5}$, and $CaCO_3$ intermetallic compounds. This reduced the dislocation movement and refined grain structure, resulting in improved mechanical and corrosion properties.
2. The addition of 1.5% NdO to the Mg-matrix improved the microhardness by 23.26% more than that of pure Mg. Moreover, the UTS and UCS values of MH1.5N were, respectively, 46.56 and 44.37% more than pure Mg. The Orowan loop mechanism and Hall–Petch relation were responsible for improved mechanical properties.
3. The surface roughness of the developed samples seems to improve by 89.5 and 20% more than MH1N and MH2N, respectively. Similarly, the contact angle values of the developed composites were in the order MH1.5N (86) > MH2N (78) > MH1N (62.4). The absence of intergranular cracking and large pores developed in the other samples were the prominent reasons for the decrease in roughness, whereas higher water retention led to increased hydrophobicity.
4. The corrosion rate was improved along with reduced hydrogen evolution in the sample with the addition of 1.5% NdO. Although the corrosion values were higher in the case of electrochemical testing than those in the weight-loss method, similar trends were obtained for corrosion rates.

6 Future work

The current study has been focused on mechanical and in vitro corrosion analysis; however, to mitigate the trade-off between strength and biocompatibility of the proposed composites, several biological evaluations will be performed in further studies.

Acknowledgement: The authors thank the Department of Physics and Materials Science, Thapar Institute of Engineering and Technology, Patiala, India, for assisting in composite fabrication and processing. The authors also acknowledge the support provided by the Thapar Institute of Engineering and Technology, Patiala, India, for this research.

Conflict of interest: The authors declare no conflict of interest.

References

[1] Wang J, Wu Y, Li H, Liu Y, Bai X, Chau W, et al. Magnesium alloy based interference screw developed for ACL reconstruction attenuates peri-tunnel bone loss in rabbits. Biomaterials. 2018;157:86–97. doi: 10.1016/j.biomaterials.2017.12.007.

[2] Chen Y, Lin S, Sun Y, Pan X, Xiao L, Zou L, et al. Translational potential of ginsenoside Rb1 in managing progression of osteoarthritis. J Orthop Transl. 2016;6:27–33. doi: 10.1016/j.jot.2016.03.001.

[3] Lui PPY, Lee YW, Mok TY, Cheuk YC. Local administration of alendronate reduced peri-tunnel bone loss and promoted graft-bone tunnel healing with minimal systemic effect on bone in contralateral knee. J Orthop Res. 2013;31:1897–906. doi: 10.1002/jor.22442.

[4] He J, Fang J, Wei P, Li Y, Guo H, Mei Q, et al. Cancellous bone-like porous Fe@Zn scaffolds with core-shell-structured skeletons for biodegradable bone implants. Acta Biomater. 2021;121:665–81. doi: 10.1016/j.actbio.2020.11.032.

[5] Chen J, Tan L, Yu X, Etim IP, Ibrahim M, Yang K. Mechanical properties of magnesium alloys for medical application: A review. J Mech Behav Biomed Mater. 2018;87:68–79. doi: 10.1016/j.jmbbm.2018.07.022.

[6] Liu J, Bian D, Zheng Y, Chu X, Lin Y, Wang M, et al. Comparative in vitro study on binary Mg-RE (Sc, Y, La, Ce, Pr, Nd, Sm, Eu, Gd, Tb, Dy, Ho, Er, Tm, Yb and Lu) alloy systems. Acta Biomater. 2020;102:508–28. doi: 10.1016/j.actbio.2019.11.013.

[7] Gao L, Chen RS, Han EH. Solid solution strengthening behaviors in binary Mg-Y single phase alloys. J Alloy Compd. 2009;472:234–40. doi: 10.1016/j.jallcom.2008.04.049.

[8] Radha R, Sreekanth D. Mechanical and corrosion behaviour of hydroxyapatite reinforced Mg-Sn alloy composite by squeeze casting for biomedical applications. J Magnes Alloy. 2020;8:452–60. doi: 10.1016/j.jma.2019.05.010.

[9] Chia TL, Easton MA, Zhu SM, Gibson MA, Birbilis N, Nie JF. The effect of alloy composition on the microstructure and tensile properties of binary Mg-rare earth alloys. Intermetallics (Barking). 2009;17:481–90. doi: 10.1016/j.intermet.2008.12.009.

[10] Knapek M, Zemková M, Greš A, Jablonská E, Lukáč F, Král R, et al. Corrosion and mechanical properties of a novel biomedical WN43 magnesium alloy prepared by spark plasma sintering. J Magnes Alloy. 2021;9:853–65. doi: 10.1016/j.jma.2020.12.017.

[11] Parande G, Manakari V, Sharma Kopparthy SD, Gupta M. A study on the effect of low-cost eggshell reinforcement on the immersion, damping and mechanical properties of magnesium–zinc alloy. Compos B Eng. 2020;182:107650. doi: 10.1016/j.compositesb.2019.107650.

[12] Kujur MS, Manakari V, Parande G, Prasadh S, Wong R, Mallick A, et al. Development of rare-earth oxide reinforced magnesium nanocomposites for orthopaedic applications: A mechanical/immersion/biocompatibility perspective. J Mech Behav Biomed Mater. 2021;114:104162. doi: 10.1016/j.jmbbm.2020.104162.

[13] Zawadzki M, Kępiński L. Synthesis and characterization of neodymium oxide nanoparticles. J Alloy Compd. 2004;380:255–9. doi: 10.1016/j.jallcom.2004.03.053.

[14] Pramanik S, Agarwal AK, Kumar Agarwal A, Rai KN. Development of high strength hydroxyapatite for hard tissue replacement. Trends Biomater Artif Organs. 2005;19(1):46–51.

[15] Wang X, Chen G, Yang W, Hussain M, Wang C, Wu G, et al. Effect of Nd content on microstructure and mechanical properties of Grf/Al composite. Mater Sci Eng A. 2011;528:8212–7. doi: 10.1016/j.msea.2011.07.039.

[16] Diffo Kaze A, Maas S, Hoffmann A, Pape D. Mechanical strength assessment of a drilled hole in the contralateral cortex at the end of the open wedge for high tibial osteotomy. J Exp Orthop. 2017;4(23):1–19. doi: 10.1186/s40634-017-0098-0.

[17] Sanjari M, Farkoosh AR, Shalchi Amirkhiz B, He Y, Javaid A, Kabir AS, et al. The role of the Zn/Nd ratio in the microstructural evolution of the Mg-Zn-Nd system during static recrystallization: Grain boundary partitioning of solutes. Scr Mater. 2017;134:1–5. doi: 10.1016/j.scriptamat.2017.01.033.

[18] Khaskhoussi A, Calabrese L, Patané S, Proverbio E. Effect of chemical surface texturing on the superhydrophobic behavior of micro–nano-roughened AA6082 surfaces. Materials. 2021;14(23):7161. doi: 10.3390/ma14237161.

[19] Chen K, Xie X, Tang H, Sun H, Qin L, Zheng Y, et al. In vitro and in vivo degradation behavior of Mg–2Sr–Ca and Mg–2Sr–Zn alloys. Bioact Mater. 2020;5:275–85. doi: 10.1016/j.bioactmat.2020.02.014.

[20] Zhang E, Yang L, Xu J, Chen H. Microstructure, mechanical properties and bio-corrosion properties of Mg-Si(-Ca, Zn) alloy for biomedical application. Acta Biomater. 2010;6:1756–62. doi: 10.1016/j.actbio.2009.11.024.